Oblique proton fire hose instability in the expanding solar wind: Hybrid simulations

Petr Hellinger[1,2] and Pavel M. Trávníček[2,1]

Abstract. Oblique fire hose instability is investigated using hybrid simulations for proton betas of the order of one and for proton parallel temperatures sufficiently greater than the perpendicular ones. The simulations confirm previous simulation results showing that this instability has a self-destructing properties and efficiently reduces the proton temperature anisotropy. A parametric study using one-dimensional standard hybrid simulations shows that stronger changes in the temperature anisotropy and stronger wave emissions appear for larger initial temperature anisotropies. An ideal, slow plasma expansion, modelled by a two-dimensional hybrid expanding box simulation, leads to a generation of proton temperature anisotropy. The anisotropy leads first to destabilization of the dominant parallel fire hose which interacts mainly with minor supra-Alfvénic protons whereas the evolution of core protons is determined by the expansion. Consequently, the effective anisotropy is only slightly reduced and the system eventually becomes unstable with respect to the oblique fire hose instability. The oblique fire hose strongly scatters the protons and removes the anisotropy disrupting the parallel fire hose. An important portion of the fluctuating wave energy is dissipated to protons and only long-wavelength waves remains in the system. The system with a low wave activity then develops again larger temperature anisotropies and the evolution repeats itself. It is concluded that both parallel and oblique proton fire hose instabilities constrain the proton temperature anisotropy in the expanding solar wind with the latter one constituting a final frontier for the anisotropy. These results give a possible explanation of some apparent discrepancies between observations and linear predictions. In addition, a simple bounded anisotropy model is developed to include some of the kinetic effects of the fire hose instabilities in fluid models.

1. Introduction

Proton velocity distribution functions in the solar wind strongly differ from the Maxwellian shape [cf., *Marsch et al.*, 1982] and may be sources of free energies for kinetic instabilities. These instabilities constitute limits on possible distribution shapes. The statistically significant data set of the WIND/SWE experiment [*Kasper et al.*, 2002, 2006] presents strong evidences of such a limiting role of instabilities. The data show clear signatures of constraints on the proton temperature anisotropies $T_{\perp p}/T_{\|p}$ (where $T_{\perp p}$ and $T_{\|p}$ are the proton perpendicular and parallel temperatures, respectively) ordered by the proton parallel beta $\beta_{\|p}$. These constraints are compatible with the theoretical marginal stability conditions for the mirror and oblique fire hose instabilities in the plasma consisting of isotropic Maxwellian electrons and bi-Maxwellian protons [*Hellinger et al.*, 2006]. Moreover, observations by *Bale and Kasper* [2008] show enhanced transverse magnetic fluctuations near the marginal stability region of the oblique fire hose as well as compressional magnetic fluctuations near the marginal stability region of mirror instability. However, the observed constraints are not compatible the theoretical marginal stability conditions of the linearly dominant instabilities, the proton cyclotron instability and the parallel fire hose (for the Maxwellian electrons, bi-Maxwellian protons). This disagreement between these observations and the linear prediction may be due to the assumptions of the plasma composition (and other parameters) used for the linear calculations; for example, on the linear level in the case of $T_{\perp p} > T_{\|p}$ a presence of a small abundance of alpha particles in the plasma [commonly observed in the solar wind, cf., *Kasper et al.*, 2007] may strongly attenuate the proton cyclotron instability in favor of the mirror instability [*Price et al.*, 1986].

The linear analysis is not a sufficient tool to understand he formation of the proton distribution functions in the expanding solar as this is a dynamic nonlinear processes. The observed temperature anisotropies (and in general departures from the Gaussian distribution) are determined by a competition between the mechanisms that drive them and the mechanisms that reduce them. In the expanding solar wind with a dominant radial magnetic field the expansion tends to drive the anisotropy $T_{\perp p} < T_{\|p}$. On the other hand, the turbulence/wave activity may heat in the perpendicular direction trough the cyclotron resonance [cf., *Hollweg and Isenberg*, 2002] which leads to the opposite anisotropy $T_{\perp p} > T_{\|p}$. Furthermore, Coulomb collisions reduce the temperature anisotropy and, finally, for sufficient anisotropies the kinetic instabilities set in. Helios observations [*Marsch et al.*, 1982] show that $T_{\perp p}/T_{\|p}$ decreases with the distance between 0.3 and 1 AU (especially for a fast solar wind) and the plasma approaches regions unstable with respect the fire hose instabilities [*Matteini et al.*, 2007].

Hybrid expanding box simulations [*Hellinger et al.*, 2003; *Matteini et al.*, 2006] that model the interaction between the expansion and the ion kinetic instabilities indicate for $\beta_{\|p} \sim 1$ that the parallel fire hose interacts mainly with minor supra-Alfvénic protons whereas the evolution of core protons is determined by the expansion. Consequently, the effective anisotropy is only slightly reduced and the system may become unstable with respect to the oblique fire hose instability. In this paper we extend the work of *Hellinger et al.* [2003] and *Matteini et al.* [2006] on the competition between the expansion and the proton fire hose instabilities. The paper is organised as follows: section 2 gives a short overview of the linear and nonlinear properties of the parallel and oblique fire hose instabilities. Section 3.1 presents a parametric study of one-dimensional (1-D) hybrid simulations of the oblique fire hose. Section 3.2 presents results of a two-dimensional (2-D) hybrid expanding box simulation. Section 4 introduces a simple fluid bounded anisotropy model that mimic the effect of the two fire hose on the proton temperature anisotropy. Finally, section 5 summarizes the present results.

[1]Institute of Atmospheric Physics, AS CR, Prague, Czech Republic
[2]Astronomical Institute, AS CR, Prague, Czech Republic

0148-0227/08/2008JA013416$9.00

2. Brief overview of the fire hose instabilities

In the low frequency, long wave-length limit [*Tajiri*, 1967] of the linearized Vlasov-Maxwell equation on can get a threshold of the (fluid) fire hose instability in the form

$$\beta_\parallel - \beta_\perp > 2 \tag{1}$$

where $\beta_\parallel$ and $\beta_\perp$ are the total parallel and perpendicular plasma beta, respectively. However, a numerical solution of the linearized Vlasov-Maxwell equation in a plasma consisting of Maxwellian electrons and bi-Maxwellian protons predicts existence of (at least) two kinetic electromagnetic instabilities. First one is a propagating instability with a maximum growth rate at the parallel direction with respect to the magnetic field, here termed parallel (proton) fire hose [*Quest and Shapiro*, 1996; *Farrugia et al.*, 1998; *Gary et al.*, 1998]. This instability drives proton whistler waves which are essentially transverse (with respect to the ambient magnetic field) and have nearly circular right-handed polarization. They have frequencies around the proton cyclotron frequency and wave lengths around the proton inertial length. Second one is a non propagating instability with a maximum growth rate at an oblique direction, here termed oblique (proton) fire hose [*Hellinger and Matsumoto*, 2000]. This instability drives linearly polarized transverse waves with wave lengths around the proton inertial length.

The numerical approach makes a determination of the threshold condition for the two instabilities difficult. Therefore, instead of searching the threshold condition, it is more convenient to solve a marginal stability condition [cf., *Gary et al.*, 1998] $\gamma_\mathrm{m} = \gamma_0$ (where γ_m is the maximum growth rate for given plasma parameters) for some small value of γ_0. One can get the approximate marginal stability conditions by fitting the equation $\gamma_\mathrm{m} = 10^{-3}\Omega_p$ with an analytical formula with only few fitting parameters [*Gary et al.*, 1998; *Hellinger et al.*, 2006]: for the parallel fire hose one can get

$$\frac{T_{\perp p}}{T_{\parallel p}} \simeq 1 - \frac{0.47}{(\beta_{\parallel p} - 0.59)^{0.53}} \tag{2}$$

whereas for the oblique fire hose one can get

$$\frac{T_{\perp p}}{T_{\parallel p}} \simeq 1 - \frac{1.4}{(\beta_{\parallel p} + 0.11)^{1.0}} \tag{3}$$

within the parameter range

$$0.1 < \beta_{\parallel p} < 30 \text{ and } 0.1 < T_{\perp p}/T_{\parallel p} < 1$$

. Note that the two instabilities are active even below the fluid threshold, Equation (1), i.e., even for

$$\frac{T_{\perp p}}{T_{\parallel p}} > 1 - \frac{2}{\beta_{\parallel p}}. \tag{4}$$

This disagreement is explained by the fact that these kinetic instabilities drives waves with short wave-lengths (comparable to proton inertial length) where the low frequency, long wave-length approximation used for the derivation of Equation (1) is not applicable.

The parallel fire hose drives ion whistler waves with the real frequency about Ω_p. This instability is resonant with protons [for $\beta_{\parallel p} < 25$, see *Gary et al.*, 1998] through the anomalous cyclotron resonance

$$\omega - k_\parallel v_\parallel = -\Omega_p. \tag{5}$$

The oblique fire hose drives non propagating oblique, transverse linearly polarized waves which result from a dispersion change of the standard propagating left-handed Alfvén waves in a plasma with the proton temperature anisotropy $T_{\perp p} < T_{\parallel p}$ [*Hellinger and Matsumoto*, 2000]. In our previous work we have erroneously assumed that the oblique fire hose is non-resonant. It turns out that the oblique fire hose is an instability resonant with protons through the cyclotron resonances

$$\omega - k_\parallel v_\parallel = \pm\Omega_p. \tag{6}$$

It interesting to note that the oblique proton fire hose has many properties, including the resonant ones, analogous to those of the non propagating oblique electron fire hose [*Li and Habbal*, 2000; *Gary and Nishimura*, 2003].

The linear dispersion predicts that the parallel fire hose is dominant for lower betas, $\beta_{\parallel p} \lesssim 4$, whereas the oblique one is dominant for higher $\beta_{\parallel p}$. However, the two instabilities have similar growth rates for a wide range of plasma parameters and their nonlinear competition is an open question as their nonlinear properties of the two instabilities (inferred from numerical simulations) are quite different. *Gary et al.* [1998] and *Matteini et al.* [2006] showed that that the parallel fire hose (for weak growth rates) saturates in a quasilinear manner. The instability drives the ion whistler waves that saturate at marginal stability and lead to an important perpendicular diffusion in the resonant region (which appears typically for parallel velocities above the Alfvén velocity). On the other hand, the oblique fire hose has a self-destructing behavior and may grow even when the parallel fire hose is saturated. The oblique fire hose drives the non propagating waves which scatter protons in the perpendicular direction (in the resonant region around the Alfvén velocity). This scattering leads to the dispersion change of the driven waves to the standard propagating Alfvén waves which are strongly damped. Some part of the fluctuating energy survives through an inverse cascade towards longer wavelengths and less oblique angles [*Hellinger and Matsumoto*, 2000, 2001].

3. Simulation results

3.1. Standard 1-D hybrid simulations

Let us start with standard 1-D hybrid simulation of the oblique proton fire hose instability. For these numerical simulations we use a modified version of the 1-D hybrid code developed by *Matthews* [1994]. In this code, electrons are considered as a massless, charge neutralizing fluid, with a constant temperature; ions are described by a particle-in-cell model and are advanced by a leapfrog scheme that requires the fields to be known at half time steps ahead of the particle velocities. This is achieved by advancing the current density to this time step with only one computational pass through the particle data at each time step. The particle leapfrog advance is based on the Boris' implicit scheme with the electromagnetic field at the particle position obtained from the mesh points by linear weighting. The particle contribution to the current density at the relevant mesh points is evaluated with linear weighting, as well, followed by smoothing over three points. No smoothing is performed on the electromagnetic fields, and the resistivity is set to zero in Ohm's law. The magnetic field is advanced in time with a modified midpoint method, which allows time substepping for the advance of the field.

In this section we investigate results of a set of 1-D standard hybrid simulations with different initial plasma parameters, $\beta_{\parallel p}$ and $T_{\perp p}/T_{\parallel p}$ (see Table 1) giving the same maximum growth rate $\gamma_\mathrm{m} = 5 \cdot 10^{-3}\Omega_p$. For each case we chose the angle θ_m (between the simulation x-direction and the ambient magnetic field $\boldsymbol{B}_0$) to be the angle between $\boldsymbol{B}_0$ and the wave vector of the most unstable mode $\boldsymbol{k}_\mathrm{m}$ (k_m being its amplitude).

For these standard 1-D simulations there are 2048 grid points in x-direction with the spatial resolution $\Delta x = 0.25c/\omega_p$ and there are 131,072 macroparticles per cell. The time step is $\Delta t = 2 \cdot 10^{-2}/\Omega_p$ while the field is advanced with $\Delta t_B = \Delta t/4$. Electrons have $\beta_e = 1$ and the standard periodic boundary conditions are used.

Table 1. Initial conditions for the set of 1-D standard hybrid simulations

Run #	$\gamma_\mathrm{m}/\Omega_p$	$\beta_{\parallel p}$	$T_{\perp p}/T_{\parallel p}$	$k_\mathrm{m}c/\omega_p$	θ_m
1		1.5	0.134	0.714	56.1°
2		2	0.332	0.498	47.7°
3	$5 \cdot 10^{-3}$	4	0.659	0.306	40.8°
4		8	0.828	0.208	38.8°
5		16	0.913	0.147	38.6°

A typical evolution of the 1-D standard hybrid simulation is shown in Figure 1 which shows the results of run 1 (see Table 1). Figure 1 shows (left top) a gray scale plot of B_z as a function of time and x (only a part of the simulation box is shown). (right top) The fluctuating magnetic energy $\delta B^2/B_0^2$ as function of time. (left bottom) The proton temperature anisotropy $T_{\perp p}/T_{\parallel p}$ as a function of time. (bottom right) The parallel proton beta $\beta_{\parallel p}$ a function of time. Figure 1 shows that the wave energy slowly grow initially and the generated waves are non propagating. The magnetic energy saturates and decays and the generated waves becomes propagating. The temperature anisotropy strongly decreases, $T_{\perp p}/T_{\parallel p}$ increases, and $\beta_{\parallel p}$ decreases.

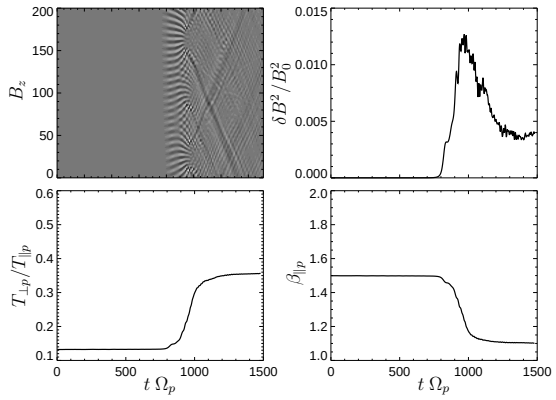

Figure 1. Evolution in run 1 (see Table 1): (left top) Gray scale plot of B_z as a function of time and x (only a part of the simulation box is shown). (right top) The fluctuating magnetic energy $\delta B^2/B_0^2$ as function of time. (left bottom) The proton temperature anisotropy $T_{\perp p}/T_{\parallel p}$ as a function of time. (bottom right) The parallel proton beta $\beta_{\parallel p}$ a function of time.

Figure 2 shows results of run 1, the proton distribution function at (left) $t = 1000/\Omega_p$ and (right) $t = 1500/\Omega_p$ as contour plots.

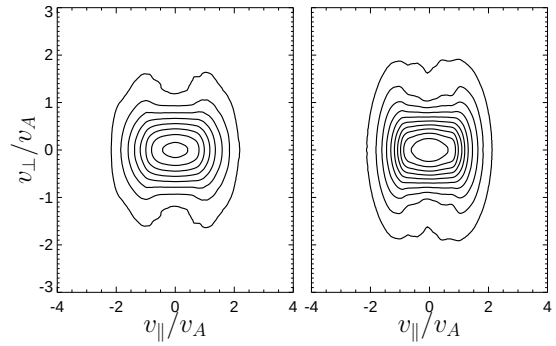

Figure 2. Contour plots of the proton distribution function $f(v_\parallel, v_\perp)$ in run 1 (see Table 1) at (left) $t = 1000/\Omega_p$ and (right) $t = 1500/\Omega_p$.

Figure 2 evidences strong cyclotron diffusion of the protons with $v_\parallel \sim v_A$ and small $v_\perp$ towards higher $v_\perp$. A more detailed inspection of the proton distribution function indicate also a signature of the Landau resonance, a weak parallel heating of protons with $v_\parallel \lesssim v_A$ [cf., *Hellinger and Trávníček*, 2006].

Figure 3 shows results of the set of the standard 1-D hybrid simulations (with parameters given in Table 1). Left panel shows paths in $(\beta_{\parallel p}, T_{\perp p}/T_{\parallel p})$ from the initial conditions (empty circles) to the final conditions (full circles). The solid curve denotes the relation $\gamma_{\rm m} = 5 \cdot 10^{-3}\Omega_p$. For comparison, the dotted curve shows the fluid threshold, Equation (4). Right panel of Figure 3 displays the maximum (full circles) and final (empty circles) fluctuating magnetic energy $\delta B^2/B_0^2$ as a function of the initial $\beta\|\ p$.

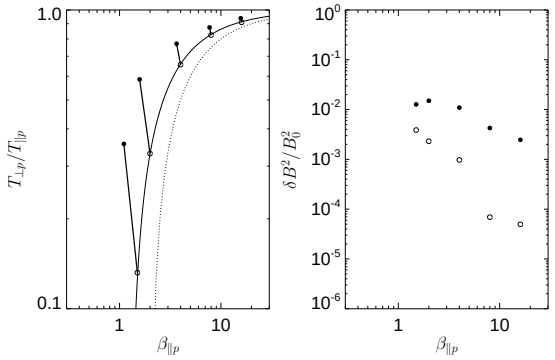

Figure 3. Standard 1-D hybrid simulations: (left) Paths in $(\beta_{\parallel p}, T_{\perp p}/T_{\parallel p})$ from the initial conditions (empty circles) to the final conditions (full circles). The solid curve denotes the relation $\gamma_{\rm m} = 5 \cdot 10^{-3}\Omega_p$. The dotted curve shows the fluid threshold (4). (right) Maximum (full circles) and final (empty circles) fluctuating magnetic energy $\delta B^2/B_0^2$ as a function of the initial $\beta\|\ p$.

Figure 3 (left panel) shows that stronger changes in the temperature anisotropy appear for lower betas and stronger initial anisotropies. Figure 3 (right panel) shows that the maximum and final fluctuating magnetic energy $\delta B^2/B_0^2$ tends be stronger for stronger initial anisotropy (smaller $T_{\perp p}/T_{\parallel p}$ corresponding to greater $\beta_{\parallel p}$).

3.2. Expanding box simulation

In standard hybrid simulations the system starts in the unstable region whereas in the solar wind the system starts in the stable region and the expansion drives the temperature anisotropy [cf., *Matteini et al.*, 2007]. To study the response of the plasma to a slow expansion we use the expanding box model [*Grappin et al.*, 1993] implemented to the hybrid code by *Matthews* [1994]. The expanding box simulations can model both the anisotropy formation from expansion and its relaxation via fire hose instabilities. In this hybrid expanding box (HEB) model [*Liewer et al.*, 2001; *Hellinger et al.*, 2003] the expansion is described as an external force. One assumes a solar wind with a constant radial velocity U at a radial distance R. Transverse scales (with respect to the radial direction) of a small portion of plasma, co-moving with the solar wind velocity, increase with time $y, z \propto (1 + t/t_e)y, z$ where $t_e = R/U$ is a characteristic time of the expansion. The expanding box uses these co-moving coordinates, the physical transverse scales of the simulation box increase with time [see *Hellinger and Trávníček*, 2005, for detailed description of the code] and the standard periodic boundary conditions are used.

The characteristic spatial and temporal units used in the model are c/ω_{p0} and $1/\Omega_{p0}$ respectively, where c is the speed of light, $\omega_{p0} = (n_0 e^2/m_p\epsilon_0)^{1/2}$ is the initial proton plasma frequency, and $\Omega_{p0} = eB_0/m_p$ is the initial proton gyrofrequency (B_0: the initial magnitude of the ambient magnetic field $\boldsymbol{B}_0$, n_0 is the initial density, e and m_p are the proton electric charge and mass, respectively; finally, ϵ_0 is the dielectric permittivity of vacuum). We use the spatial resolution $\Delta x = \Delta y = c/\omega_{p0}$, and there are $1,024$ particles per cell. Fields and moments are defined on a 2-D (periodic) x–y grid with dimensions 256×256. Protons are advances using the Boris' scheme with a time step $\Delta t = 0.02/\Omega_{p0}$, while the magnetic field $\boldsymbol{B}$ is advanced with a smaller time step $\Delta t_B = \Delta t/10$. The initial ambient magnetic field is directed along the radial, x direction, $\boldsymbol{B}_0 = (B_0, 0, 0)$, and we impose a continuous expansion in y and z directions with a characteristic time $t_e = 10^4/\Omega_{p0}$.

For the strictly radial magnetic field the expansion leads to a decrease of the ambient density and magnitude of the magnetic field as $(1+t/t_e)^{-2}$. The double adiabatic prediction of the proton temperature anisotropy and parallel beta in the expanding box is

$$\frac{T_{\parallel p}}{T_{\perp p}} \propto \beta_{\parallel p} \propto \left(1+\frac{t}{t_e}\right)^2. \quad (7)$$

The evolution in the 2-D HEB simulation is shown in Figure 4 as a path in the space $(\beta_{\parallel p}, T_{\perp p}/T_{\parallel p})$ by solid curve; the empty circles denote the initial conditions whereas the full circles denotes the end of a first oscillation. The dashed contours shows the linear prediction in a homogeneous plasma with bi-Maxwellian protons: the maximum growth rate (in units of Ω_p) as a function of $\beta_{\parallel p}$ and $T_{\perp p}/T_{\parallel p}$ for (left) the parallel proton fire hose and (right) the oblique one.

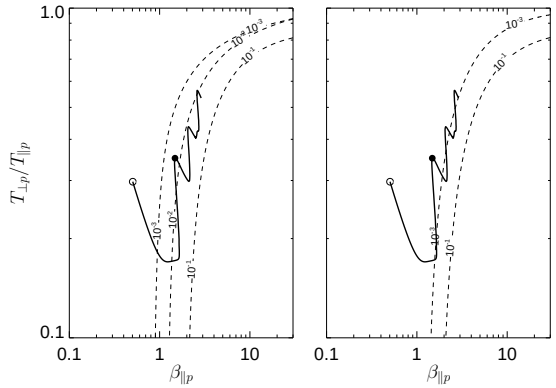

Figure 4. Evolution in 2-D HEB simulation: Path in the space $(\beta_{\parallel p}, T_{\perp p}/T_{\parallel p})$ is shown by solid curve; the empty circles denote the initial conditions whereas the full circles denotes the end of a first oscillation. The dashed contours shows the linear prediction in a homogeneous plasma with bi-Maxwellian protons: the maximum growth rate (in units of Ω_p) as a function of $\beta_{\parallel p}$ and $T_{\perp p}/T_{\parallel p}$ for (left) the parallel proton fire hose and (right) the oblique one.

The evolution of the simulated expanding exhibit oscillations in the space $(\beta_{\parallel p}, T_{\perp p}/T_{\parallel p})$; let us look in detail at the first period between the beginning, denoted by the empty circle, and the full circle. This period may be divided in three phases. During the first phase, the system follows the double-adiabatic prediction; this phase ends around the first crossing of the $\gamma_{\rm m} = 10^{-3}\Omega_p$ contour of the parallel fire hose, at $t \sim 0.4t_e$ (Figure 4, left panel). This double adiabatic evolution is modified during the second phase when the system enters the region unstable with respect to the parallel fire hose. The system is able to get relatively far into the instable region so that in enters the unstable region with respect to the oblique fire hose. During the third phase the system then rapidly jumps back to the region stable to with respect to the oblique fire hose. This phase starts close to the first crossing of the $\gamma_{\rm m} = 10^{-3}\Omega_p$ contour of the oblique fire hose (Figure 4, right panel), at about $t = 0.8t_e$ and it ends at about $t = 0.9t_e$ (denoted by the full circles on Figure 4). Afterwards, another oscillation starts with the proton anisotropy increasing in a nearly double-adiabatic manner. The oscillation between the unstable and stable regions (with respect to the oblique fire hose) repeats two more times, although with smaller variations of the temperature anisotropy $T_{\perp p}/T_{\parallel p}$. This evolution indicate a presence of the parallel fire hose instability during the second phase and of the oblique fire hose instability during the third phase.

In order to verify a presence of the two instabilities let us look at the wave spectra in the simulation. The evolution of the wave spectra is displayed in Figure 5 which shows (top left) the distance from the marginal stability $\Gamma_{\rm of}$ (with respect to the oblique fire hose) defined from Equations (3) as

$$\Gamma_{\rm of} = \frac{1.4}{(\beta_{\parallel p}+0.11)^{1.0}} + \frac{T_{\perp p}}{T_{\parallel p}} - 1 \quad (8)$$

as a function of time (dashed curve shows the double-adiabatic prediction). (top right) Fluctuating magnetic energy $\delta B^2/B_0^2$ as a function of time; dashed curve shows the fluctuating magnetic energy $\delta B^2/B_0^2$ at oblique angles, $|\theta_{kB}| > 20^\circ$. (bottom left) Gray scale plot of the fluctuating magnetic energy δB^2 as a function of time and the wave vector kc/ω_p. (bottom right) Gray scale plot of the fluctuating magnetic energy δB^2 as a function of time and angle θ_{kB}. Note that the inertial length increases with time

$$c/\omega_p \propto n^{-1/2} \propto 1 + t/t_e$$

so that the physical resolution is time dependent. Along the non expanding x-axis we have $\Delta x\omega_p/c \propto 1/(1+t/t_e)$ whereas for the expanding y-axis we have $\Delta y\omega_p/c$ is constant as the increase of c/ω_p is compensated by the expansion. Consequently, the spatial resolution of quasi-parallel waves with a wavelength about c/ω_p is initially somewhat poor but becomes better later when the parallel fire hose sets in.

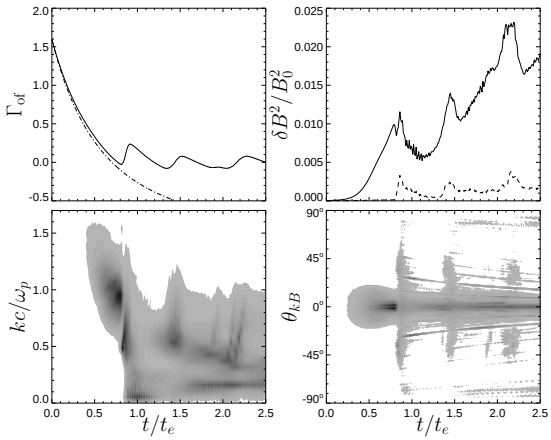

Figure 5. Evolution in 2-D HEB simulation: (top left) Distance from the marginal stability $\Gamma_{\rm of}$ (Equation (8)) as a function of time (dash-dotted curve shows the double-adiabatic prediction). (top right) Fluctuating magnetic energy $\delta B^2/B_0^2$ as a function of time (dashed curve shows the fluctuating magnetic energy $\delta B^2/B_0^2$ at oblique angles, $|\theta_{kB}| > 20^\circ$). (bottom left) Gray scale plot of the fluctuating magnetic energy δB^2 as a function of time and the wave vector kc/ω_p. (bottom right) Gray scale plot of the fluctuating magnetic energy δB^2 as a function of time and angle θ_{kB}.

Figure 5 confirms the existence of a wave activity in the simulation, generated by the two instabilities. Most of the fluctuating magnetic energy $\delta B^2/B_0^2$ appears at quasi-parallel angles $|\theta_{kB}| \lesssim 20^\circ$. During the first phase, $t \lesssim 0.3t_e$, there is no discernible fluctuating magnetic energy and the system follows the double-adiabatic evolution. During the second phase, $0.3t_e \lesssim t \lesssim 0.8t_e$, waves driven by the parallel fire hose slowly appear with the maximum intensity at the parallel propagation and the wave vector about ω_p/c; during this phase the system path start to deviates from the double-adiabatic evolution. During the short third phase, $0.8t_e \lesssim t \lesssim 0.9t_e$, waves driven by the oblique fire hose rapidly appear at wide range of oblique angles with wave vectors $\sim 0.6\omega_p/c$. These waves also rapidly disappear and are partly damped to protons, partly cascade to longer wavelength and less oblique angles. The proton scattering due to the oblique fire hose leads to damping of an important portion of wave energy contained in the waves due to the parallel fire hose. The cycle of the

three phases then repeats itself. During these cycles, the wave energy $\delta B^2/B_0^2$ at quasi-parallel angles increases; these wave consist partly of waves driven by the parallel fire hose, partly of waves resulting from the inverse cascade from oblique fire hose.

The waves generated by the two instabilities interact with protons in a different way. The ion whistler waves generated by the parallel fire hose instability interact through the anomalous cyclotron resonance whereas, the initially non propagating waves, transformed to standard Alfvén waves during the nonlinear evolution of the oblique fire hose interact with protons through the cyclotron and Landau resonances. Figure 6 displays the proton distribution function $f(v_\parallel, v_\perp)$ at (left) $t = 0.8t_e$, (i.e. at the end of the second phase) and (right) $t = 1.2t_e$, (i.e. at the time of the local minimum of $\delta B^2/B_0^2$, see Figure 5) as contour plots.

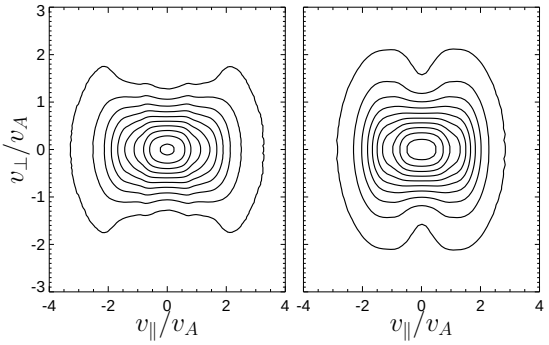

Figure 6. Contour plots of the proton distribution function $f(v_\parallel, v_\perp)$ at (left) $t = 0.8t_e$ and (right) $t = 1.2t_e$.

Figure 6 (left panel) shows the result of the interaction between protons and the parallel fire hose driven ion whistler waves: affected are mainly particles with high parallel velocities $|v_\parallel| \sim 2v_A$ which are required for the anomalous cyclotron resonance [*Matteini et al.*, 2006]. Figure 6 (right panel) shows mainly the effect of the proton scattering by the oblique fire hose driven waves. This scattering affects strongly particles with $|v_\parallel| \sim v_A$. Detailed analysis also indicate a weak parallel heating of the core protons $|v_\parallel| < V_A$.

The presented simulations results are only weakly dependent on the numerical parameters. We have performed additional simulations with different resolutions and box sizes and we have obtained quantitatively similar results. On the other hand, the characteristic expansion time t_e is an important parameter. For a faster expansion, smaller t_e, the system enters further to the theoretically unstable regions in the space $(\beta_{\parallel p}, T_{\perp p}/T_{\parallel p})$ [cf., *Matteini et al.*, 2006; *Hellinger and Trávníček*, 2005] but the overall evolution of the system is qualitatively similar. With the present computational capabilities we cannot perform simulations with a slower expansion. We expect similar results even for a slower expansion. It is, however, possible that for a sufficiently slow expansion the evolution is governed only by the parallel fire hose instability [*Matteini et al.*, 2006].

4. Bounded anisotropy model

Here we propose a bounded anisotropy model [*Denton et al.*, 1994], as a possible way how to include kinetic wave-particle interaction due to the two fire hose instabilities following for fluid modeling. The behavior of the parallel and perpendicular temperatures in the double-adiabatic approximation is given by

$$\begin{aligned}\left(\frac{dT_{\perp p}}{dt}\right)_{\rm CGL} &= T_{\perp p}\frac{d\log B}{dt}\\ \left(\frac{dT_{\parallel p}}{dt}\right)_{\rm CGL} &= -2T_{\parallel p}\frac{d\log(B/n)}{dt}.\end{aligned} \quad (9)$$

where B and n are the magnitude of magnetic field and the proton number density, respectively. Effect of wave-particle interaction on the fluid level may be described by an energy-conserving isotropization term that couples the two temperatures

$$\begin{aligned}\frac{dT_{\perp p}}{dt} &= \left(\frac{dT_{\perp p}}{dt}\right)_{\rm CGL} + \nu\left(T_{\parallel p} - T_{\perp p}\right)\\ \frac{dT_{\parallel p}}{dt} &= \left(\frac{dT_{\parallel p}}{dt}\right)_{\rm CGL} + 2\nu\left(T_{\perp p} - T_{\parallel p}\right)\end{aligned} \quad (10)$$

where the isotropization frequency ν is assumed to be a sum of contributions corresponding to each instability, $\nu = \nu_{\rm pf} + \nu_{\rm of}$. The contribution of the parallel fire hose is chosen to be simply proportional to the distance from the marginal stability $\Gamma_{\rm pf}$ (with respect to the parallel fire hose) defined from Equations (2) as

$$\Gamma_{\rm pf} = \frac{0.47}{(\beta_{\parallel p} - 0.59)^{0.53}} + \frac{T_{\perp p}}{T_{\parallel p}} - 1. \quad (11)$$

The contribution is chosen in this simple form:

$$\nu_{\rm pf}(\beta_{\parallel p}, T_{\perp p}/T_{\parallel p}) = \begin{cases} 0 & \text{for } \Gamma_{\rm pf} \le 0\\ \nu_{\rm pf0}\Gamma_{\rm pf} & \text{for } \Gamma_{\rm pf} > 0\end{cases} \quad (12)$$

For the oblique fire hose we chose the isotropization frequency $\nu_{\rm of}$ with a memory. Initially, in the stable region, for $\Gamma_{\rm of} < 0$ (where $\Gamma_{\rm of}$ is defined in Equation (8)) we set $\nu_{\rm of} = 0$. Inside the unstable region, $\Gamma_{\rm of} > 0$, $\nu_{\rm of}$ is for simplicity assumed to be constant

$$\nu_{\rm of}(\beta_{\parallel p}, T_{\perp p}/T_{\parallel p}) = \nu_{\rm of0} \quad (13)$$

whereas outside, for $\Gamma_{\rm of} < 0$, $\nu_{\rm of}$ decreases with a characteristic time τ

$$\frac{d\nu_{\rm of}}{dt} = -\frac{\nu_{\rm of}}{\tau}. \quad (14)$$

We take $\nu_{\rm pf0} = 6 \cdot 10^{-5}\Omega_{p0}$, $\nu_{\rm of0} = 10^{-3}\Omega_{p0}$ and $\tau = 200/\Omega_{p0}$, the same initial parameters ($\beta_{\parallel p} = 0.5$ and $T_{\perp p}/T_{\parallel p} = 0.3$), and the same evolution as in the hybrid expanding box simulation, namely the proton density and the ambient magnetic field decrease as $(1 + t/t_e)^{-2}$ with $t_e = 10^4/\Omega_{p0}$. For these conditions the evolution determined by Equation (10) exhibits a behavior similar to that in the hybrid expanding box simulation. Results of this bounded anisotropy model are shown in Figure 7. Figure 7 shows a path the space $(\beta_{\parallel p}, T_{\perp p}/T_{\parallel p})$ obtained from the integration of Equation (10) in the same format as in Figure 4. Results of the bounded anisotropy model are in a qualitative agreement with the results of the hybrid expanding box model. It is, however, important to note that the results of this simple bounded anisotropy model are relatively sensitive to the free parameters. Therefore, the chosen values of these parameters cannot be considered as general and need to be adjusted to given situation.

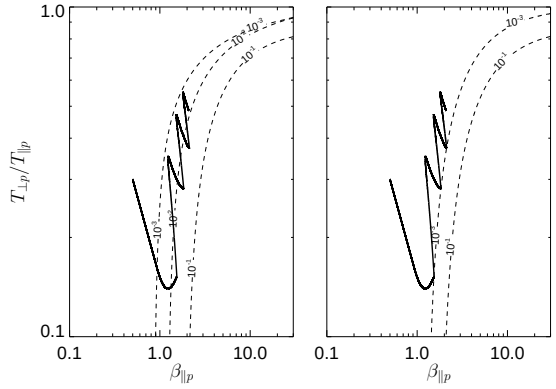

Figure 7. Results from the bounded anisotropy model: Path in the space $(\beta_{\|p}, T_{\perp p}/T_{\|p})$. The dashed contours shows the linear prediction in a homogeneous plasma with bi-Maxwellian protons: the maximum growth rate (in units of Ω_p) as a function of $\beta_{\|p}$ and $T_{\perp p}/T_{\|p}$ for (left) the parallel proton fire hose and (right) the oblique one.

5. Conclusion

The presented 1-D standard hybrid simulations confirm the previous simulation results on the nonlinear evolution of the oblique proton fire hose instability. This instability has a self-destructing properties; the non propagating waves generated during the initial phase of the instability transform themselves to propagating waves owing to dispersive properties of the oblique fire hose. The propagating, standard Alfvén waves are strongly damped mainly through the cyclotron resonance and partly through the Landau one; consequently, protons are efficiently heated in the perpendicular direction. Only a part of the Alfvén-wave magnetic fluctuating energy remains on large spatial scales owing to the inverse cascade. The parametric study of these simulations shows that stronger changes in the temperature anisotropy and stronger wave emissions appear for larger initial temperature anisotropies (and lower parallel proton betas).

Using the 2-D hybrid expanding box simulation we have investigated the role of the parallel and oblique fire hose instabilities ($\beta_{\|p} \sim 1$) in a slowly expanding plasma with the characteristic expansion time $t_e = 10^4/\Omega_p$ (which is close to its realistic values in the solar wind at 1 AU which are typically of the order of $10^5/\Omega_p$) The simulated ideal slow expansion leads to the double-adiabatic evolution of proton temperatures; for the strictly radial magnetic field this evolution generates a continuous decrease of $T_{\perp p}/T_{\|p}$ as well as a continuous increase of $\beta_{\|p}$. The system becomes unstable first with respect to the parallel fire hose. This instability generates low-frequency, ion whistler waves and their presence makes the evolution to depart from the double-adiabatic prediction. The parallel fire hose has a quasi-linear saturation, the whistler waves interact through the anomalous cyclotron resonance with mainly the supra-Alfvénic protons which are minor for $\beta_{\|p} \sim 1$. The major core protons are nearly double adiabatic, and, consequently, the system becomes unstable with respect to the oblique fire hose instability that efficiently heats the protons and remove the proton anisotropy owing to the self-destructing nonlinear evolution. The oblique instability disrupts the quasi-linear balance of the whistler waves and an important portion of whistler wave energy is dissipated to protons; only long-wavelength whistler waves remains in the system as well as long-wavelength Alfvén waves resulting from the inverse cascade. The system with a low wave activity then follows a double-adiabatic-like behavior and the evolution repeats itself.

The fluctuating wave energy $\delta B^2/B_0^2$ increases with time (and $\beta_{\|p}$) apart from the oscillatory decreases induced by the oblique fire hose. Similarly, 1-D hybrid expanding box simulations [*Matteini et al.*, 2006], (which allow only the parallel fire hose) exhibit a continuous increase of the fluctuating wave energy $\delta B^2/B_0^2$ with time (and $\beta_{\|p}$). These results are compatible with the observation results of *Bale and Kasper* [2008] which show enhanced transverse magnetic fluctuations near the marginal stability regions of the two fire hose instabilities and the observed $\delta B^2/B_0^2$ increases with $\beta_{\|p}$.

In concluding, the present results together with the results of *Matteini et al.* [2006] and with observations by *Bale and Kasper* [2008] indicate that both parallel and oblique proton fire hose instabilities constrain the proton temperature anisotropy in the expanding solar wind with the latter one constituting a final frontier for the anisotropy. These results explain the apparent discrepancy between the linear prediction and observations for $T_{\perp p} < T_{\|p}$ [*Hellinger et al.*, 2006]. The kinetic fire hoses (unstable even for $\beta_{\|} - \beta_{\perp} < 2$, i.e., below the fluid threshold) have likely a similar role in other weakly collisional space plasmas [e.g., *Sharma et al.*, 2006; *Schekochihin et al.*, 2008]. Following *Denton et al.* [1994] we have developed a simple bounded anisotropy model that includes some effects of the kinetic instabilities for fluid modelling [cf., *Samsonov et al.*, 2007].

Acknowledgments. Authors acknowledge the Czech grants GAAV IAA300420702 and IAA300420602. The simulations have been performed on Amalka supercomputing facility at IAP, ASCR.

References

Bale, S. D., and J. C. Kasper (2008), Magnetic fluctuation power and compressibility near proton temperature anisotropy instability thresholds in the solar wind, *Phys. Rev. Lett.*, *?*, in preparation.

Denton, R. E., B. J. Anderson, S. P. Gary, and S. A. Fuselier (1994), Bounded anisotropy fluid model for ion temperatures, *J. Geophys. Res.*, *99*, 11,225–11,241.

Farrugia, C. J., F. T. Gratton, G. Gnavi, and K. W. Ogilvie (1998), On the possible excitation of electromagnetic ion cyclotron waves in solar ejecta, *J. Geophys. Res.*, *103*, 6543–6550.

Gary, S. P., and K. Nishimura (2003), Resonant electron firehose instability: Particle-in-cell simulations, *Phys. Plasmas*, *10*, 3571–3576.

Gary, S. P., H. Li, S. O'Rourke, and D. Winske (1998), Proton resonant firehose instability: Temperature anisotropy and fluctuating field constraints, *J. Geophys. Res.*, *103*, 14,567–14,574.

Grappin, R., M. Velli, and A. Mangeney (1993), Nonlinear-wave evolution in the expanding solar wind, *Phys. Rev. Lett.*, *70*, 2190–2193.

Hellinger, P., and H. Matsumoto (2000), New kinetic instability: Oblique Alfvén fire hose, *J. Geophys. Res.*, *105*, 10,519–10,526.

Hellinger, P., and H. Matsumoto (2001), Nonlinear competition between the whistler and Alfvén fire hoses, *J. Geophys. Res.*, *106*, 13,215–13,218.

Hellinger, P., and P. Trávníček (2005), Magnetosheath compression: Role of characteristic compression time, alpha particle abundances and alpha/proton relative velocity, *J. Geophys. Res.*, *110*, A04210, doi: 10.1029/2004JA010687.

Hellinger, P., and P. Trávníček (2006), Parallel and oblique proton fire hose instabilities in the presence of alpha/proton drift: Hybrid simulations, *J. Geophys. Res.*, *111*, A01107, doi:10.1029/2005JA011318.

Hellinger, P., P. Trávníček, A. Mangeney, and R. Grappin (2003), Hybrid simulations of the expanding solar wind: Temperatures and drift velocities, *Geophys. Res. Lett.*, *30*, 1211, doi:10.1029/2002GL016409.

Hellinger, P., P. Trávníček, J. C. Kasper, and A. J. Lazarus (2006), Solar wind proton temperature anisotropy: Linear theory and WIND/SWE observations, *Geophys. Res. Lett.*, *33*, L09101, doi: 10.1029/2006GL025925.

Hollweg, J. V., and P. A. Isenberg (2002), Generation of the fast solar wind: A review with emphasis on the resonant cyclotron interaction, *J. Geophys. Res.*, *107*, 1147, doi:10.1029/2001JA000270.

Kasper, J. C., A. J. Lazarus, and S. P. Gary (2002), Wind/SWE observations of firehose constraint on solar wind proton temperature anisotropy, *Geophys. Res. Lett.*, *29*, 1839, doi:10.1029/2002GL015128.

Kasper, J. C., A. J. Lazarus, J. T. Steinberg, K. W. Ogilvie, and A. Szabo (2006), Physics-based tests to identify the accuracy of solar wind ion measurements: A case study with the Wind Faraday cups, *J. Geophys. Res.*, *111*, A03105, doi:10.1029/2005JA011442.

Kasper, J. C., M. Stevens, A. J. Lazarus, J. T. Steinberg, and K. W. Ogilvie (2007), The solar wind helium abundance as a function of speed and heliographic latitude, *Astrophys. J.*, *660*, 901–910.

Li, X., and S. R. Habbal (2000), Electron kinetic firehose instability, *J. Geophys. Res.*, *105*, 27,377–27,386.

Liewer, P. C., M. Velli, and B. E. Goldstein (2001), Alfvén wave propagation and ion cyclotron interaction in the expanding solar wind: One-dimensional hybrid simulations, *J. Geophys. Res.*, *106*, 29,261–29,281.

Marsch, E., K. H. Muhlhauser, R. Schwenn, H. Rosenbauer, W. Pilipp, and F. M. Neubauer (1982), Solar-wind protons – three-dimensional velocity distributions and derived plasma parameters measured between 0.3 AU and 1 AU, *J. Geophys. Res.*, *87*, 52–72.

Matteini, L., S. Landi, P. Hellinger, and M. Velli (2006), Parallel proton fire hose instability in the expanding solar wind: Hybrid simulations, *J. Geophys. Res.*, *111*, A10101, doi:10.1029/2006JA011667.

Matteini, L., S. Landi, P. Hellinger, F. Pantellini, M. Maksimovic, M. Velli, B. E. Goldstein, and E. Marsch (2007), The evolution of the solar wind proton temperature anisotropy from 0.3 to 2 AU, *Geophys. Res. Lett.*, *34*, L20105, doi:10.1029/2007GL030920.

Matthews, A. (1994), Current advance method and cyclic leapfrog for 2D multispecies hybrid plasma simulations, *J. Comput. Phys.*, *112*, 102–116.

Price, C. P., D. W. Swift, and L.-C. Lee (1986), Numerical simulation of nonoscillatory mirror waves at the Earth's magnetosheath, *J. Geophys. Res.*, *91*, 101–112.

Quest, K. B., and V. D. Shapiro (1996), Evolution of the fire-hose instability: Linear theory and wave-wave coupling, *J. Geophys. Res.*, *101*, 24,457–24,469.

Samsonov, A. A., O. Alexandrova, C. Lacombe, M. Maksimovic, and S. P. Gary (2007), Proton temperature anisotropy in the magnetosheath: comparison of 3-D MHD modelling with cluster data, *Ann. Geophys.*, *25*, 1157–1173.

Schekochihin, A. A., S. C. Cowley, R. M. Kulsrud, M. S. Rosin, and T. Heinemann (2008), Nonlinear growth of firehose and mirror fluctuations in astrophysical plasmas, *Phys. Rev. Lett.*, *100*, 081301.

Sharma, P., G. W. Hammett, E. Quataert, and J. M. Stone (2006), Shearing box simulations of the MRI in a collisionless plasma, *Astrophys. J.*, *637*, 952–967.

Tajiri, M. (1967), Propagation of hydromagnetic waves in collisionless plasma. II. Kinetic approach, *J. Phys. Soc. Jpn.*, *22*, 1482–1494.

P. Hellinger, Institute of Atmospheric Physics, AS CR, Prague 14131, Czech Republic. (petr.hellinger@ufa.cas.cz)

P. M. Trávníček, Astronomical Institute, AS CR, Prague 14131, Czech Republic. (trav@ig.cas.cz)